nanomaterials

MDPI

Communication

Phase-Selective Synthesis of Mo–Ta–C Ternary Nanosheets by Precisely Tailoring Mo/Ta Atom Ratio on Liquid Copper

Rong Tu [1,2,3], Hang Yang [1], Chitengfei Zhang [1,2,*], Baowen Li [1], Qingfang Xu [1], Qizhong Li [1], Meijun Yang [1] and Song Zhang [1]

[1] State Key Laboratory of Advanced Technology for Materials Synthesis and Processing, Wuhan University of Technology, Wuhan 430070, China; turong@whut.edu.cn (R.T.); deepyangsir@gmail.com (H.Y.); bwli@whut.edu.cn (B.L.); xuqingfanghed@gmail.com (Q.X.); qizhongli@whut.edu.cn (Q.L.); liyangmeijun@163.com (M.Y.); kobe@whut.edu.cn (S.Z.)

[2] Chaozhou Branch of Chemistry and Chemical Engineering Guangdong Laboratory, Chaozhou 521000, China

[3] Wuhan University of Technology Advanced Engineering Technology Research Institute of Zhongshan City, Zhongshan 528400, China

* Correspondence: zctf@foxmail.com

Abstract: Phase-selective synthesis is an effective way to expand the ultra-thin transition metal carbide family and tune its properties. Herein, a chemical vapor deposition route with specially designed substrate (Ta wire–Cu foil–Mo foil) is carried out to synthesize Mo–Ta–C ternary nanosheets with tunable phase structure. The Ta atoms diffuse on the surface of liquid copper and Mo atoms diffuse through the liquid copper to the surface, which react with the carbon atoms decomposed from the methane and form the Mo–Ta–C ternary nanosheets. By precisely tailoring the Mo/Ta ratio and growth temperature, ultrathin layered orthorhombic $(Mo_{2/3}Ta_{1/3})_2C$ nanosheets and non-layered cubic $(Mo_{0.13}Ta_{0.87})$ C nanosheets with thickness of 21 and 4 nm are selectively synthesized. The approach could pave the way for the formation of multi-component carbide nanosheets with controllable phases.

Keywords: phase-selective synthesis; Mo–Ta–C ternary nanosheets; chemical vapor deposition; Mo/Ta ratio

Citation: Tu, R.; Yang, H.; Zhang, C.; Li, B.; Xu, Q.; Li, Q.; Yang, M.; Zhang, S. Phase-Selective Synthesis of Mo–Ta–C Ternary Nanosheets by Precisely Tailoring Mo/Ta Atom Ratio on Liquid Copper. *Nanomaterials* **2022**, *12*, 1446. https://doi.org/10.3390/nano12091446

Academic Editor: Antonino Gulino

Received: 3 March 2022
Accepted: 21 April 2022
Published: 24 April 2022

1. Introduction

2D transition metal carbides (TMCs) have drawn great attention all over the world in the past few years due to the diverse physical and chemical properties, including superconductivity [1], valley polarization [2], and high catalytic activity [3,4]. Various binary TMC nanosheets (V_2C [5], Ti_2C [6], Mo_2C [7,8] Nb_4C_3 [9], Zr_3C_2 [10], etc.) synthesized by liquid exfoliation or chemical vapor deposition (CVD) have been applied in catalysis, solar cells, and microelectronics, indicating that the synthesis and property research of binary TMCs tends to be mature.

In order to tune the properties of 2D TMCs further, defects, dangling bonds, and alloy elements are introduced (Table S1) [11–13]. However, the introduction of defects and dangling bonds could tune the performance slightly and weaken the intrinsic performance of binary carbides significantly [14,15]. While the introduction of alloy elements leads to improving the performance fundamentally [16,17]. For example, the microhardness of the ternary carbides $(Ti_{0.4}Hf_{0.6})C$ is almost twice that of HfC [16]. Mo_2TiC_2 and $Mo_2Ti_2C_3$ reveal substantially higher electrochemical behavior compared to Mo_2C [17]. The synthesis of binary TMC nanosheets by CVD methods has made some progress in the past few years. Zhang et al. [18] directly obtained the self-aligned vanadium carbide with face-centered cubic structure on a unique stacked substrate by a CVD method. Xu et al. [1] achieved the layered hexagonal α-Mo_2C and non-layered face-centered cubic WC on liquid copper by atmospheric pressure CVD, indicating the possibility of phase-selective synthesis for TMCs.

However, limited by the synthesis strategies, it remains difficult to synthesize the ternary 2D TMC nanosheets by CVD method so far.

Herein, a sandwich-like substrate consisting of a Ta wire, Cu foil, and Mo foil is proposed to synthesize ternary 2D Mo–Ta–C (MTC) nanosheets. The Ta atoms diffuse on the liquid copper from the Ta wire and Mo atoms diffuse through the liquid copper from the bottom Mo foil. Followed by the introduction of CH_4, C, Ta, and Mo atoms are bonded together and form the 2D MTC nanosheets on liquid copper. Ultrathin layered orthorhombic $(Mo_{2/3}Ta_{1/3})_2C$ nanosheets and non-layered cubic $(Mo_{0.13}Ta_{0.87})C$ nanosheets were selectively synthesized into triangular and polygonal geometries by adjusting the molar ratio of Mo/Ta.

2. Materials and Methods

2.1. Synthesis of Single-Crystalline $(Mo_{2/3}Ta_{1/3})_2C$ and $(Mo_{0.13}Ta_{0.87})C$

The self-made chemical vapor deposition system is utilized to synthesize carbides. A molybdenum foil (20 × 20 mm, Innochem, Beijing, China 99.99%) 50 μm in thickness, Tungsten foil (20 × 20 mm, Innochem, Beijing, China 99.99%) 50 μm in thickness, a copper foil (20 × 20 mm, Innochem, Beijing, China 99.99%) 50 μm in thickness, and a tantalum wire (20 mm, Innochem, Beijing, China 99.99%) 0.5 mm in diameter are cleaned with acetone (Innochem, Beijing, China 95%), ethanol (Innochem, Beijing, China 95%), and deionized water. The Mo foil, Cu foil, Ta wire, and W foil are stacked from the top in the order of (a) Mo wire–Cu foil–Ta foil; (b) Mo wire and Ta wire–Cu foil–W foil; (c) Ta wire–Cu foil–Mo foil. After that, the furnace (Tianjin Zhonghuan Lab Furnace Co., Ltd., Tianjin, China) is heated to 1090–1170 °C within 90 min under the flow of Ar (300 sccm, 99.999%) and H_2 (300 sccm, 99.999%) and held there for 30 to 60 min. Finally, with introducing the methane flow (0.1–2 sccm, 99.999%), graphene, TaC, and single crystalline $(Mo_{2/3}Ta_{1/3})_2C$ and $(Mo_{0.13}Ta_{0.87})C$ phases were obtained on the liquid copper substrates under the different Mo/Ta ratios.

2.2. Transfer Process

A thin layer of poly (methyl methacrylate) (PMMA, weight-averaged molecular mass M_W = 600,000, 6 wt% in anisole) was first spin-coated on samples at 3000 rpm for 1 min and cured at 120 °C for 10 min. The PMMA-coated samples were then immersed in a 0.2 M $(NH_4)_2SO_4$ solution for 24 h to etch the Cu substrate. Finally, the PMMA-coated ultrathin MTC crystals were stamped onto target substrates, such as SiO_2/Si and TEM grids, and warm acetone (55 °C) was utilized to dissolve the PMMA layer and obtain clean ultrathin MTC crystals.

2.3. Characterization

Optical microscopy (OM, MX6RT, Sunny Optical Technology Co., Yuyao, China) is carried out in a reflection mode. The Bruker Multimode 8 DI (Burker, Billerica, MA, USA) in contact mode is performed for atomic force microscopy (AFM) imaging. Horiba Lab Ram HR (Horiba, Kyoto, Japan) 800 eV with 532 nm laser is performed for Raman analysis and imaging. A JEM-2100 F (JEOL, Akishima, Japan) at 200 kV is performed for high-resolution transmission electron microscopy (HRTEM) and selected-area electron diffraction (SAED).

3. Results

The phase diagrams of Cu-Mo and Cu-Ta are shown in Figure S1, indicating that the Cu cannot form intermetallic compounds with Ta and Mo [19,20]. Thus, the pure Ta and Mo wire, foil, or block could diffuse on liquid copper surface without damaging the atomic-level flat surface. When the temperature rises up to 1090 °C, Ta and Mo atoms would diffuse on or though the liquid copper and bond with carbon atoms decomposed from CH_4. Several different stacking orders have been conducted: (a) Mo wire–Cu foil–Ta foil (Figure 1a); (b) Mo wire and Ta wire–Cu foil–W foil (Figure 1d); (c) Ta wire–Cu foil–Mo foil (Figure 1g).

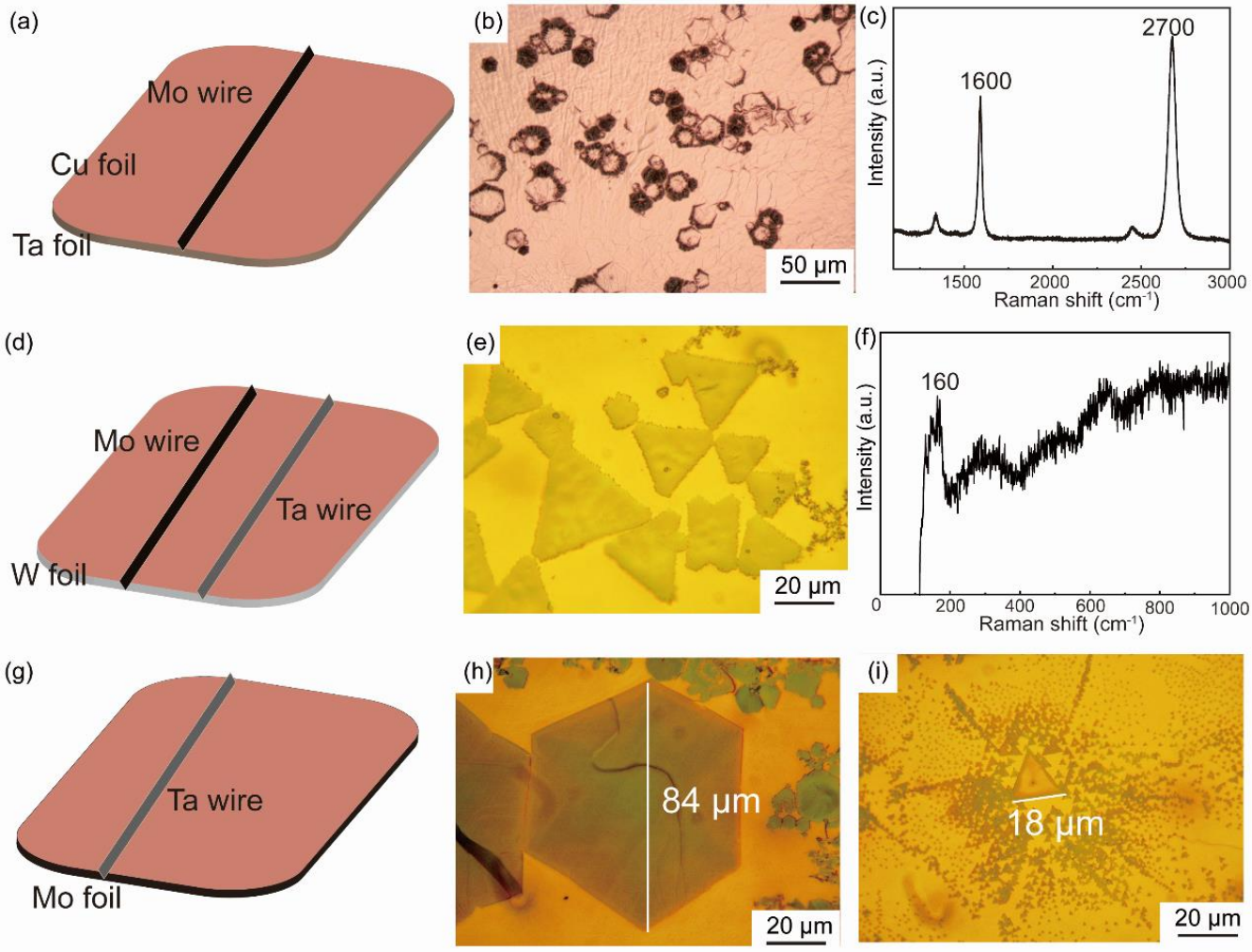

Figure 1. Several different stacking orders of transition metallic source: (**a**) Mo wire–Cu foil–Ta foil, (**b**) optical image and (**c**) Raman spectrum of graphene corresponding to (**a**). (**d**) Mo wire and Ta wire–Cu foil–W foil, (**e**) optical image and (**f**) Raman spectrum of TaC corresponding to (**d**). (**g**) Ta wire–Cu foil–Mo foil, (**h**) optical image of polygonal and (**i**) triangular nanosheet corresponding to (**g**).

For the order (a), EDS measurements indicate (Figure S2) no Mo and Ta was identified in the detection limit, and only graphene was obtained on the liquid copper (Figure 1b,c). For the order (b), W foil acts as support for liquid copper and triangular tantalum carbide nanosheets were achieved (Figure 1e,f), indicating that Ta could effectively diffuse on the surface of liquid copper and Mo was on the opposite. Based on the above results, the order (c) was carried out. Polygonal (Figure 1h) and triangular (Figure 1i) nanosheets were grown separately under the diffusion time of 30 and 60 min. The schematic diagram of the growth process is shown in Figure S3.

4. Discussion

In order to further identify the crystal structure and chemical composition of the two kinds of nanosheets, HRTEM, SAED, and EDS (Figure 2) are performed. Figure 2b–d are the EDS mapping of the crystal in Figure 2a, indicating that the crystal is composed of Ta, Mo, and C. The SAED pattern (Figure 2e) collected from Figure 2a is referred to the simple orthorhombic form (JCPDS no. 31-0871) with a space group of Pbcn(60), suggesting the chemical formula is $(Ta_xMo_{1-x})_2C$. The atomic resolution image (Figure 2f) is observed under the [100] zone axis. The two different planes with the lattice spacing of 0.263 and

0.258 nm is consistent with the (021) and (002) plane. In order to confirm the ratio of Mo to Ta precisely, EDS point scan is performed at the nine selected points marked in Figure 2a. The ratio of Mo to Ta collected from the nine points is approximately 2:1, demonstrating the chemical formula is $(Ta_{1/3}Mo_{2/3})_2C$. Figure 2i is the atomic model of a unit cell of $(Ta_{1/3}Mo_{2/3})_2C$ with the lattice parameters of a = 0.4754 nm, b = 0.5241 nm, c = 0.6076 nm, $\alpha = 90°$, $\beta = 90°$, $\gamma = 90°$.

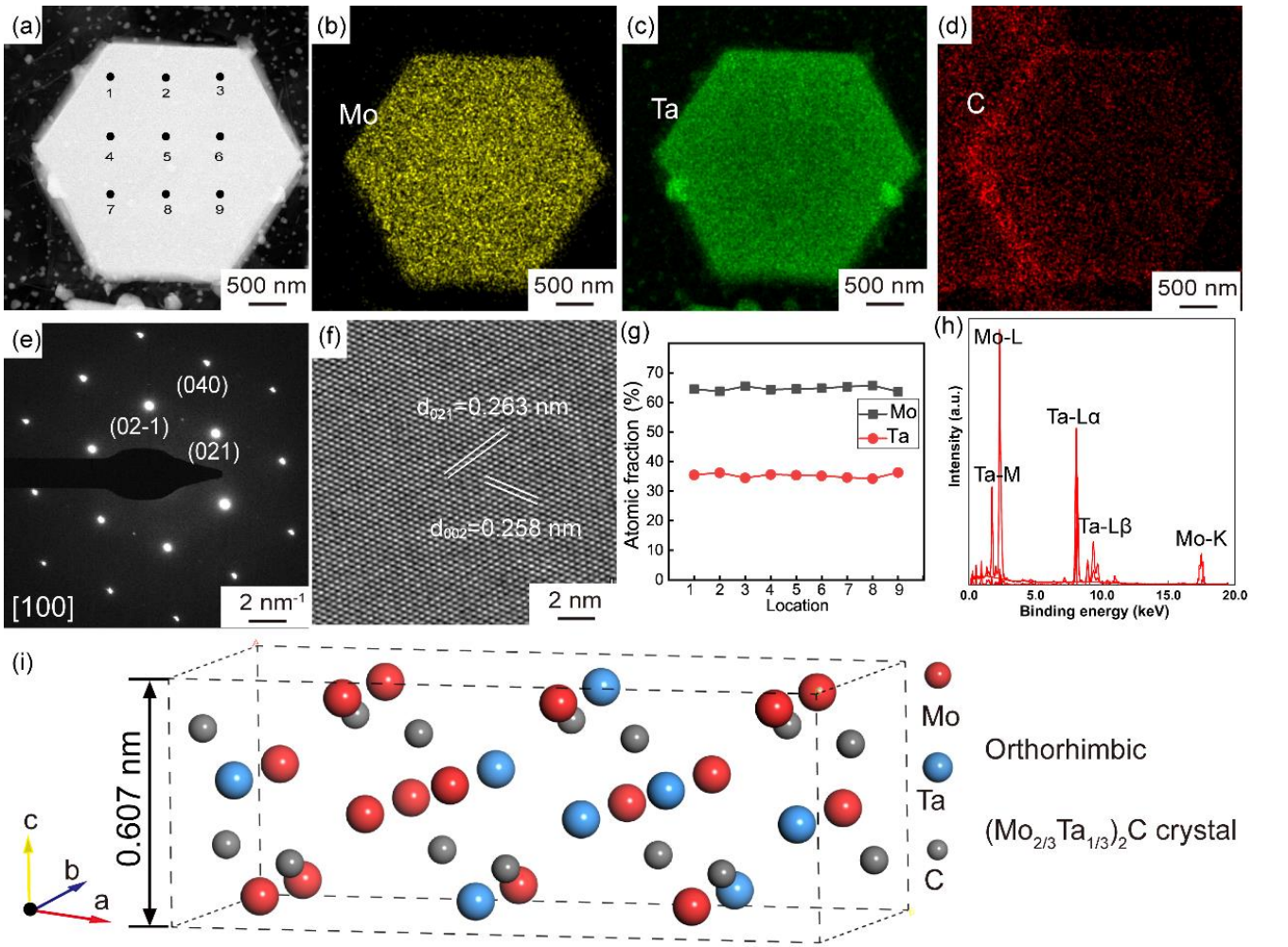

Figure 2. TEM images of polygonal MTC crystal (**a**) and corresponding EDS elemental mapping of Mo (**b**), Ta (**c**), and C (**d**). SAED pattern along [100] zone axis (**e**) and HRTEM image of a polygonal crystal (**f**). Atomic fraction of Mo and Ta in the polygonal crystal of (**a**). (**g**) Based on EDS spectrum (**h**). (**i**) Crystallographic structure of orthorhombic $(Mo_{2/3}Ta_{1/3})C$.

Figure 3a shows a low-magnification high-angle annular dark-field (HAADF)-STEM image of a triangular nanosheet crystal. Mo, Ta, and C are uniformly distributed across the whole sheet (Figure 3b–d), indicating the uniform chemical composition. Figure 3e shows the SAED pattern along the [1-1-1] zone axis. The two different planes with the lattice spacing of 0.157 and 0.090 nm are consistent with the (220) and (422) plane. These lattice parameters are consistent with cubic TaC (JCPDS no. 35-0801). EDS point scan is performed at the six selected points marked in Figure 3a. The ratio of Mo to Ta collected from the six points is approximately 13:87, demonstrating the chemical formula is $(Ta_{0.13}Mo_{0.87})C$. Figure 3i is the atomic model of a unit cell of $(Ta_{1/3}Mo_{2/3})_2C$ with the lattice parameters of a = 0.4455 nm, b = 0.4455 nm, c = 0.4455 nm, $\alpha = 90°$, $\beta = 90°$, $\gamma = 90°$.

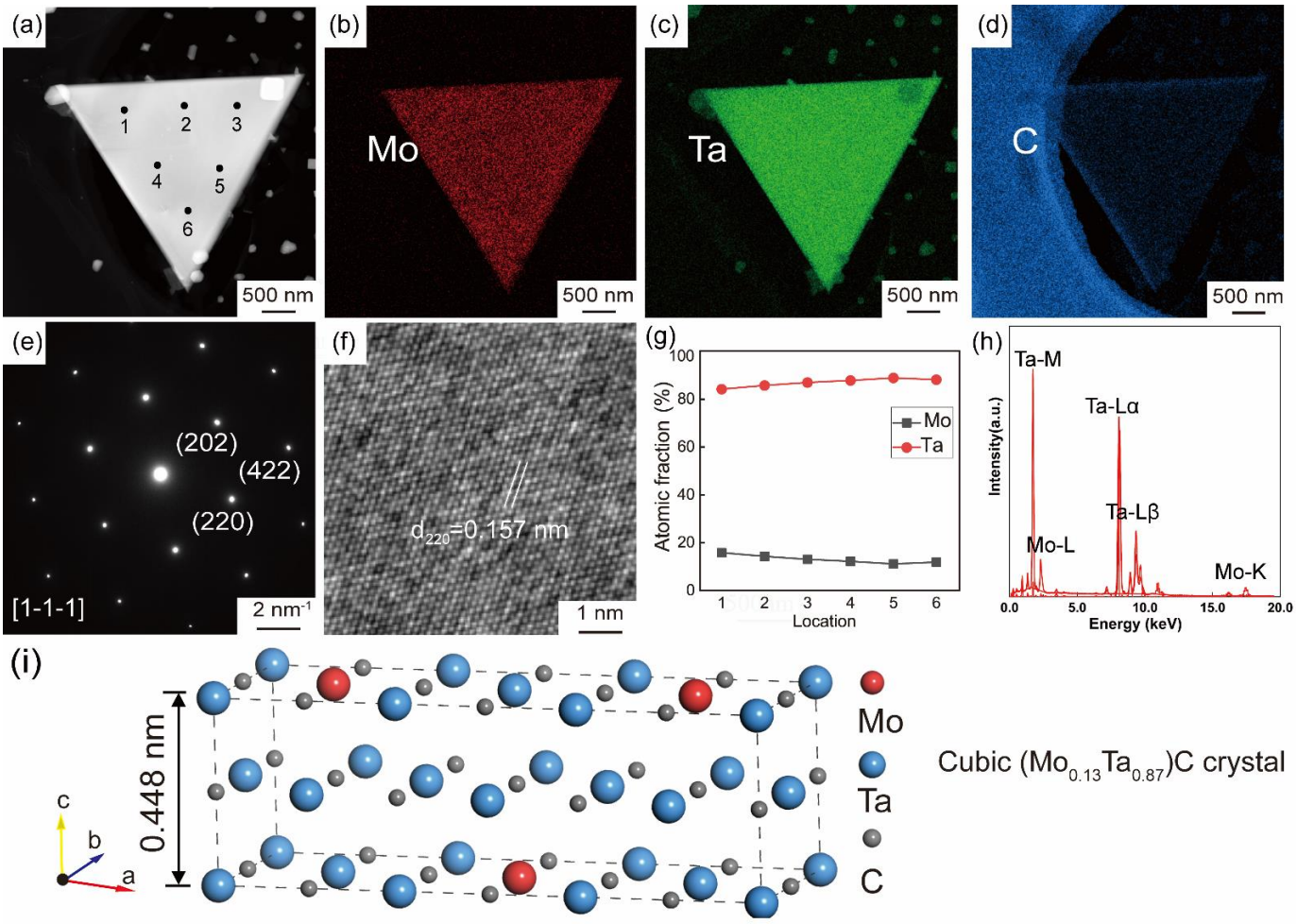

Figure 3. TEM images of triangular MTC crystal (**a**) and corresponding EDS elemental mapping of Mo (**b**), Ta (**c**), and C (**d**). SAED pattern along [1] zone axis (**e**) and HRTEM image of a triangular crystal (**f**). Atomic fraction of Mo and Ta in the triangular crystal of (**a**). (**g**) Based on EDS spectrum (**h**). (**i**) Crystallographic structure of cubic ($Mo_{0.13}Ta_{0.87}$)C.

As shown in Raman spectra (Figure 4a), the orthorhombic MTC phase has two prominent peaks at the peak positions of 143 and 649 cm^{-1}. The cubic MTC phase has two characteristic peaks located at 130 and 632 cm^{-1} in Figure 4e, respectively. The peak position at 130 cm^{-1} is attributed to the Ta-C bond, and the 143 cm^{-1} peak is related to the typical Mo-C bond of B_{3g} Raman modes [21]. The peak near 632 cm^{-1} is a typical peak of TMCs, as seen at NbC [22], TaC [23], and Mo_2C [21,24]. Meanwhile, Figure 4c,g depict the Raman mappings of the orthorhombic and cubic phases, demonstrating the uniformity of the two phases. The size of polygonal nanosheet is 84 µm (in Figure 1f) in length and 21 nm in thickness (Figure 4d). Another phase is typically triangular with a size of 15 µm and thickness of 4 nm (Figure 4h).

Figure 5 shows the effect of temperature and Mo/Ta atomic fraction on the growth of orthorhombic and cubic MTC. The Mo/Ta ratio is controlled by the diffusion time.

Both orthorhombic and cubic MTC nanosheets were synthesized at 1090–1170 °C. Orthorhombic MTC nanosheets were obtained at Mo/Ta atomic fraction of Ta from 10% to 40%. Cubic MTC nanosheets were obtained at Mo/Ta atomic fraction of Ta from 60% to 90%. Mo_2C nanosheets were obtained (Figure S4) without the Ta wire. The corresponding optical images are shown in Figure S5. When the atomic percentage of Ta was low (10–20%), the orthorhombic MTC nanosheets tended to form larger single nanosheets with lower

nucleation density (Figure S5a–e). When the atomic percentage of Ta was high (80–90%), cubic MTC nanosheets tended to aggregate together (Figure S5k–p).

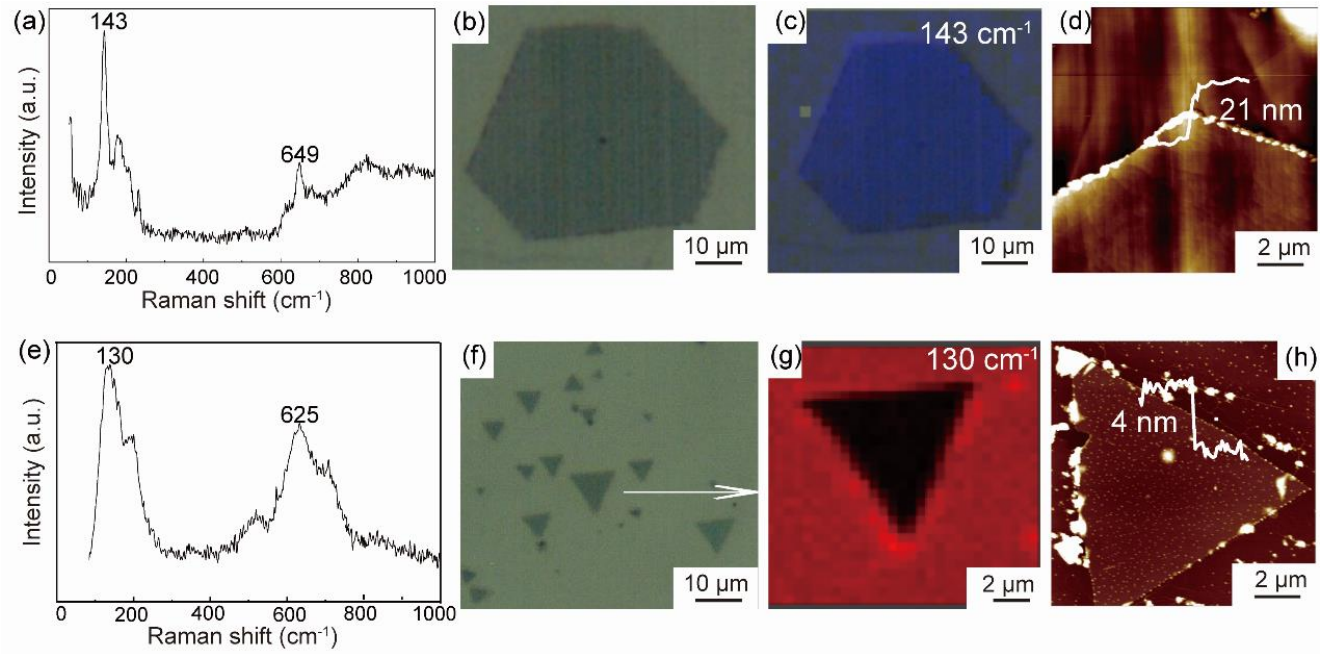

Figure 4. Raman spectra (**a**,**e**), optical images (**b**,**f**), Raman mapping (**c**,**g**) and AFM images (**d**,**h**) of orthorhombic (**a**–**d**) and cubic (**e**–**h**) MTC phases.

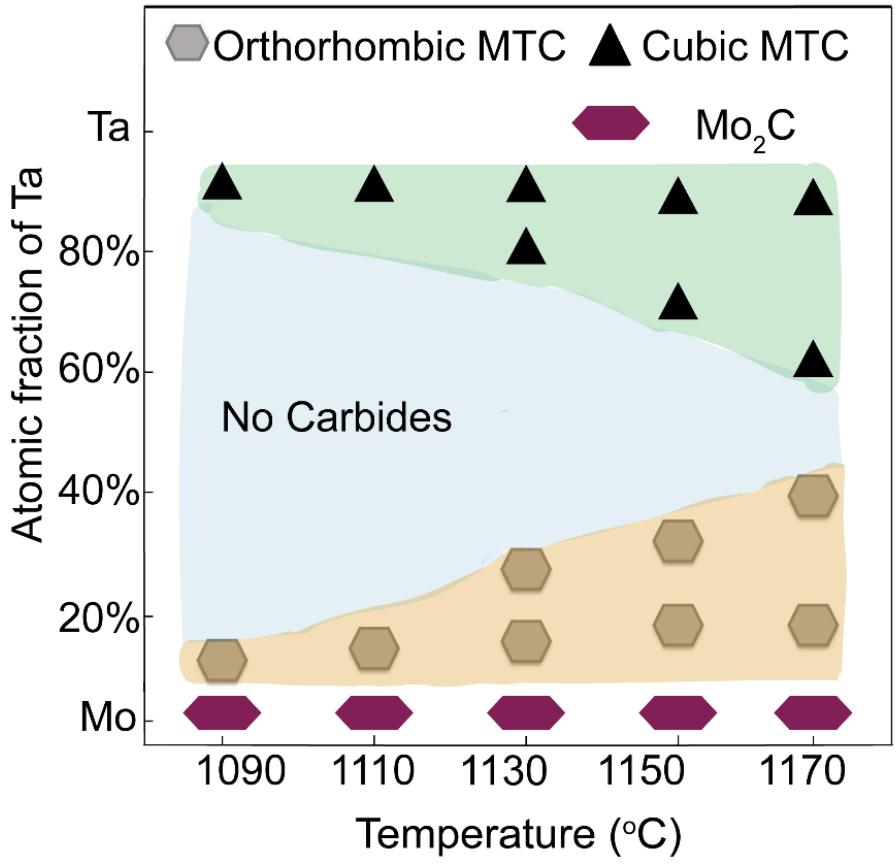

Figure 5. Effect of temperature and Mo/Ta atomic fraction on the growth of orthorhombic and cubic MTC.

5. Conclusions

A phase selective CVD method with the special stacked order of Ta wire–Cu foil–Mo foil was developed to control the synthesis of orthorhombic and cubic MTC nanosheets with high crystallinity on liquid copper. The maximum size of orthorhombic MTC nanosheets reached 84 μm grown at Mo/Ta ratio of 9:1. While the cubic MTC nanosheets had the largest size of 18 μm grown at Mo/Ta ratio of nearly 1:9, demonstrating that the growth of MTC is deeply influenced by the Mo/Ta molar ratio. This study paves a new way for the synthesis of multiphase 2D nanosheets with controllable phase.

Supplementary Materials: The following supporting information can be downloaded at: https://www.mdpi.com/article/10.3390/nano12091446/s1, Figure S1: Phase diagrams of Cu-Mo and Cu-Ta; Figure S2: SEM and EDS of Mo wire and Ta foil after diffusion; Figure S3: The schematic diagram of orthorhombic and cubic MTC growth processes; Figure S4: Optical image and Raman of Mo_2C; Figure S5: The optical images of orthorhombic and cubic MTC with different Mo/Ta atomic fraction of Ta and temperature. The scale bar is 20 μm. Table S1: Main characterizations of different synthetic technologies for TMCs [1,20,25–35].

Author Contributions: Conceptualization, B.L. and Q.X.; Methodology, S.Z.; Validation, C.Z. and R.T.; Formal analysis, Q.L. and M.Y.; Data curation, H.Y.; Writing—original draft preparation, H.Y.; Visualization, S.Z. and B.L.; Supervision, C.Z. and R.T.; Project administration, R.T.; Writing—review and editing, C.Z. All authors have read and agreed to the published version of the manuscript.

Funding: This research was funded by the Guangdong Major Project of Basic and Applied Basic Research (2021B0301030001), the Key-Area Research and Development Program of Guangdong Province (2021B0707050001, 2019B121204001, 2020B010181001), the China Postdoctoral Science Foundation (2021M692492), the Chaozhou Science and Technology Project (2019PT01), the Self-innovation Research Funding Project of Hanjiang Laboratory (HJL202012A001, HJL202012A002, HJL202012A003, HJL202104A001), and the Major Science and Technology Project in Zhongshan City, Guangdong Province (2019AG029). This work was also supported by the Joint Fund of the Ministry of Education for Pre-research of Equipment (6141A02022257), the Science Challenge Project (no. TZ2016001), the National Natural Science Foundation of China (nos. 51861145306, 51872212, and 51972244), and the 111 Project (B13035). It was also supported by the International Science & Technology Cooperation Program of China (2018YFE0103600), the Technological Innovation of Hubei Province, China (2019AAA030).

Institutional Review Board Statement: Not applicable.

Informed Consent Statement: Not applicable.

Data Availability Statement: Data can be available upon request from the authors.

Conflicts of Interest: The authors declare no conflict of interest.

References

1. Xu, C.; Wang, L.B.; Liu, Z.B.; Chen, L.; Guo, J.K.; Kang, N.; Ma, X.L.; Cheng, H.M.; Ren, W.C. Large-area high-quality 2D ultrathin Mo_2C superconducting crystals. *Nat. Mater.* **2015**, *14*, 1135–1141. [CrossRef]
2. Li, S.; He, J.J.; Grajciar, L.; Nachtigall, P. Intrinsic valley polarization in 2D magnetic MXenes: Surface engineering induced spin-valley coupling. *Mater. Chem. C* **2021**, *9*, 11132–11141. [CrossRef]
3. Zhao, D.; Chen, Z.; Yang, W.J.; Liu, S.J.; Zhang, X.; Yu, Y.; Cheong, W.; Zheng, L.R.; Ren, F.Q.; Ying, G.B.; et al. MXene (Ti_3C_2) vacancy-confined single-atom catalyst for efficient functionalization of CO_2. *Am. Chem. Soc.* **2019**, *141*, 4086–4093. [CrossRef] [PubMed]
4. Zhang, J.Q.; Zhao, Y.F.; Guo, X.; Chen, C.; Dong, C.; Liu, R.; Han, C.; Li, Y.D.; Gogotsi, Y.; Wang, G.X. Single platinum atoms immobilized on an MXene as an efficient catalyst for the hydrogen evolution reaction. *Nat. Catal.* **2018**, *1*, 985–992. [CrossRef]
5. Wu, M.; Wang, B.X.; Hu, Q.K.; Wang, L.B.; Zhou, A.G. The synthesis process and thermal stability of V_2C MXene. *Materials* **2018**, *11*, 2112. [CrossRef]
6. Halim, J.; Persson, I.; Moon, E.; Kuhne, P.; Darakchieva, V.; Persson, P.; Eklund, P.; Rosen, J.; Barsoun, M. Electronic and optical characterization of 2D Ti_2C and Nb_2C (MXene) thin films. *J. Phys. Condens. Matter* **2019**, *31*, 165301. [CrossRef]
7. Geng, D.C.; Zhao, X.X.; Chen, Z.X.; Sun, W.W.; Fu, W.; Chen, J.Y.; Liu, W.; Zhou, W.; Loh, K.P. Direct synthesis of large-area 2D Mo_2C on in situ grown graphene. *Adv. Mater.* **2017**, *29*, 1700072. [CrossRef] [PubMed]

8. Zha, X.H.; Yin, J.S.; Zhou, Y.H.; Huang, Q.; Luo, K.; Lang, J.J.; Francisco, J.S.; He, J.; Du, S.Y. Intrinsic structural, electrical, thermal, and mechanical properties of the promising conductor Mo_2C MXene. *J. Phys. Chem. C* **2016**, *120*, 15082–15088. [CrossRef]
9. Ghidiu, M.; Naguib, M.; Shi, C.; Mashtalir, O.; Pan, L.M.; Zhang, B.; Yang, J.; Gogotsi, Y.; Billinge, S.J.L.; Barsoum, M.W. Synthesis and characterization of two-dimensional Nb_4C_3 (MXene). *Chem. Commun.* **2014**, *50*, 9517–9520. [CrossRef] [PubMed]
10. Zhou, J.; Zha, X.H.; Chen, F.Y.; Ye, Q.; Eklund, P.; Du, S.Y.; Huang, Q. A two-dimensional zirconium carbide by selective etching of Al_3C_3 from nano laminated $Zr_3Al_3C_5$. *Angew. Chem. Int. Ed. Engl.* **2016**, *55*, 5008–5013. [CrossRef]
11. Kamysbayev, V.; Filatov, A.S.; Hu, H.; Rui, X.; Lagunas, F.; Wang, D.; Klie, R.F.; Talapin, D.Y. Covalent surface modifications and superconductivity of two-dimensional metal carbide MXenes. *Science* **2020**, *369*, 979–983. [CrossRef]
12. Shen, Z.; Wang, Z.; Zhang, M.; Gao, M.X.; Hu, J.J.; Du, F.; Liu, Y.F.; Pan, H. A novel solid-solution MXene $(Ti_{0.5}V_{0.5})_3C_2$ with high catalytic activity for hydrogen storage in MgH_2. *Scr. Mater.* **2018**, *1*, 114–120. [CrossRef]
13. Verger, L.; Xu, C.; Natu, V.; Cheng, H.M.; Ren, W.C.; Barsoum, M.W. Overview of the synthesis of MXenes and other ultrathin 2D transition metal carbides and nitrides. Curr. Opin. *Solid State Mater Sci.* **2019**, *23*, 149–163. [CrossRef]
14. Lipatov, A.; Lu, H.; Alhabeb, M.; Anasori, B.; Gruverman, A.; Gogotsi, Y.; Sinitskii, A. Elastic properties of 2D $Ti_3C_2T_x$ MXene monolayers and bilayers. *Sci. Adv.* **2018**, *4*, eaat0491. [CrossRef]
15. Lipatov, A.; Alhabeb, M.; Lu, H.; Zhao, S.S.; Loes, M.J.; Vorobeva, N.S.; Agnese, Y.D.; Gao, Y.; Gruverman, A.; Gogotsi, Y.; et al. Electrical and elastic properties of individual single-layer $Nb_4C_3T_x$ MXene flakes. *Adv. Funct.* **2020**, *6*, 1901382. [CrossRef]
16. Subramanian, P.R.; Laughlin, D.E. The Cu-Ta (copper-tantalum) system. *Bull. Alloy Phase Diagr.* **1989**, *10*, 652–655. [CrossRef]
17. Subramanian, P.R.; Laughlin, D.E. The Cu-Mo (copper-molybdenum) system. *Bull. Alloy Phase Diagr.* **1990**, *11*, 169–172. [CrossRef]
18. Helmersson, U.; Todorova, S.; Barnett, S.A.; Sundgren, J.E.; Markert, L.C.; Greene, J.E. Growth of single-crystal TiN/VN strained-layer superlattices with extremely high mechanical hardness. *J. Appl. Phys.* **1987**, *62*, 481–484. [CrossRef]
19. Karmakar, S.; Saha-Dasgupta, T. First-principles prediction of enhanced thermoelectric properties of double transition metal MXenes: $Ti_{3-x}Mo_xC_2T_2$;(x= 0.5, 1, 1.5, 2, 2.5, T=−OH/−O/−F). *Phys. Rev. Mater.* **2020**, *4*, 124007. [CrossRef]
20. Zhang, C.; Wang, Z.G.; Tu, R.; Dong, M.D.; Li, J.; Yang, M.J.; Li, Q.Z.; Shi, J.; Li, H.W.; Ohmori, H.; et al. Growth of self-aligned single-crystal vanadium carbide nanosheets with a controllable thickness on a unique staked metal substrate. *Appl. Surf. Sci.* **2020**, *499*, 143998. [CrossRef]
21. Li, T.S.; Luo, W.J.; Kitadai, H.; Wang, X.Z.; Ling, X. Probing the domain architecture in 2D α-Mo_2C via polarized raman spectroscopy. *Adv. Mater.* **2019**, *31*, 1807160. [CrossRef]
22. Wipf, H.; Klein, M.V.; Williams, W.S. Vacancy-induced and two-phonon raman scattering in ZrC_x, NbC_x, HfC_x, and TaC_x. *Phys. Status Solidi B* **1981**, *108*, 489–500. [CrossRef]
23. Yang, J.H.; Liu, Z.J.; Wang, H.Q.; Xiao, K.S.; Guo, Q.G.; Song, J.R.; Liu, L. The reaction behavior of carbon fibers and TaC at high temperatures. *CrystEngComm* **2013**, *15*, 6928–6931. [CrossRef]
24. Kang, Z.; Zheng, Z.; Wei, H.; Zhang, Z.; Tan, X.Y.; Xiong, L.; Zhai, T.Y.; Gao, Y.H. Controlled growth of an Mo_2C-graphene hybrid film as an electrode in self-powered two-sided Mo_2C-Graphene/$Sb_2S_{0.42}Se_{2.58}$/TiO_2 photodetectors. *Sensors* **2019**, *19*, 1099. [CrossRef]
25. Chaitoglou, S.; Giannakopoulou, T.; Speliotis, T.; Speliotis, A.; Vavouliotis, A.; Trapalis, C.; Dimoulas, A. Mo2C/graphene heterostructures: Low temperature chemical vapor deposition on liquid bimetallic Sn-Cu and hydrogen evolution reaction electrocatalytic properties. *Nanotechnology* **2019**, *30*, 125401. [CrossRef]
26. Sun, W.; Wang, X.; Feng, J.; Li, T.; Huan, Y.; Qiao, J.; Ma, D. Controlled synthesis of 2D Mo_2C/graphene heterostructure on liquid Au substrates as enhanced electrocatalytic electrodes. *Nanotechnology* **2019**, *30*, 385601. [CrossRef]
27. Naguib, M.; Mashtalir, O.; Carle, J.; Presser, V.; Lu, J.; Hultman, L.; Gogotsi, Y.; Barsoum, M.W. Two-dimensional transition metal carbides. *ACS Nano* **2012**, *6*, 1322–1331. [CrossRef]
28. Zhou, J.; Zha, X.; Zhou, X.; Chen, X.; Gao, X.; Wang, S.; Shen, C.; Chen, T.; Zhi, C.; Eklund, P.; et al. Synthesis and electrochemical properties of two-dimensional hafnium carbide. *ACS Nano* **2017**, *11*, 3841–3850. [CrossRef]
29. Shuck, C.E.; Sarycheva, A.; Anayee, M.; Levitt, A.; Zhu, Y.; Uzun, S.; Gogotsi, Y. Scalable Synthesis of $Ti_3C_2T_x$ MXene. *Adv. Eng. Mater.* **2020**, *22*, 1901241. [CrossRef]
30. Maleski, K.; Ren, C.E.; Zhao, M.Q.; Anasori, B.; Gogotsi, Y. Size-dependent physical and electrochemical properties of two-dimensional MXene flakes. *ACS Appl. Mater. Interfaces* **2018**, *10*, 24491–24498. [CrossRef]
31. Tao, Q.; Dahlqvist, M.; Lu, J.; Kota, S.; Meshkian, R.; Halim, J.; Palisaitis, J.; Hultman, L.; Barsoum, M.; Persson, P.; et al. Two-dimensional Mo1.33C MXene with divacancy ordering prepared from parent 3D laminate with in-plane chemical ordering. *Nat. Commun.* **2017**, *8*, 1–7. [CrossRef] [PubMed]
32. Wu, C.; Li, J. Unique Hierarchical Mo_2C/C Nanosheet Hybrids as Active Electrocatalyst for Hydrogen Evolution Reaction. *ACS Appl. Mater. Interfaces* **2017**, *9*, 41314–41322. [CrossRef] [PubMed]
33. Jia, J.; Xiong, T.; Zhao, L.; Wang, F.; Liu, H.; Hu, R.; Chen, S. Ultrathin N-Doped Mo_2C Nanosheets with Exposed Active Sites as Efficient Electrocatalyst for Hydrogen Evolution Reactions. *ACS Nano* **2017**, *11*, 12509–12518. [CrossRef] [PubMed]
34. Wang, J.; Liu, S.; Wang, Y.; Wang, T.; Shang, S.; Ren, W. Magnetron-sputtering deposited molybdenum carbide MXene thin films as saturable absorber for passively Q-switched laser. *J. Mater. Chem. C.* **2020**, *8*, 1608–1613. [CrossRef]
35. Zhang, K.; Wen, M.; Cheng, G.; Li, X.; Meng, Q.N.; Lian, J.S.; Zheng, W.T. Reactive magnetron sputtering deposition and characterization of niobium carbide films. *Vacuum* **2014**, *99*, 233–241. [CrossRef]